Ultrafast Photooxidation of Mn(II)−Terpyridine Complexes Covalently Attached to TiO_2 Nanoparticles

Sabas G. Abuabara, Clyde W. Cady, Jason B. Baxter, Charles A. Schmuttenmaer,* Robert H. Crabtree,* Gary W. Brudvig,* and Victor S. Batista*

Department of Chemistry, Yale University, P. O. Box 208107, New Haven, Connecticut 06520-8107

Received: March 26, 2007; In Final Form: May 11, 2007

This paper reports visible-light sensitization of TiO_2 nanoparticles by surface modification with Mn(II)−terpyridine complexes, as evidenced by UV−vis spectroscopy of colloidal thin films and aqueous suspensions. Photoexcitation of the $[Mn^{II}(H_2O)_3(\text{catechol-terpy})]^{2+}/TiO_2$ (terpy = 2,2′:6,2″-terpyridine) complex, attached to the TiO_2 surface, leads to interfacial electron transfer within 300 fs as indicated by ultrafast optical pump−terahertz probe transient measurements and computational simulations. Photoinduced interfacial electron transfer is accompanied by Mn(II) → Mn(III) photooxidation. The half-time for regeneration of the Mn(II) complex is ca. 23 s (at 6 K), as monitored by time-resolved measurements of the Mn(II) EPR signal.

Introduction

Interfacial electron transfer (IET) between molecular adsorbates and semiconductor nanoparticles is a fundamental process relevant to many important applications, including solar-energy conversion by dye-sensitized solar cells,[1,2] photocatalysis,[3−6] and molecular electronics.[7,8] Most previous studies have been focused on TiO_2 nanoparticles sensitized with Ru dyes,[9,10] although IET in other semiconductor materials (e.g., ZnO, ZrO, SnO_2, and Al_2O_3)[11−19] and surface complexes based on other transition metals (e.g., Rh, Re, Os, Ga. and Zn)[9,20−24] have also been investigated. We report the first photoinduced IET between a Mn(II) coordination compound and TiO_2 nanoparticles. The importance of this initial result is that the resulting Mn(III) state is known to be a highly effective oxidant for organic compounds,[25−36] thus raising the future possibility of useful light-induced oxidation chemistry.

Light absorption by coordination compounds (e.g., $[Ru(bpy)_3]^{2+}$) has been one of the classic approaches investigated to store chemical energy.[37,38] However, low efficiencies were typically obtained due to photobleaching and fast recombination reactions.[37,39] It was subsequently discovered that intrinsically photolabile Ru−polypyridyl complexes can become extremely photostable when bound to semiconductor surfaces (e.g., colloidal TiO_2), mainly due to the highly efficient charge-separation processes triggered by photoexcitation of the surface complexes.[40−42] The underlying stabilization mechanism involves ultrafast photooxidation of the surface complexes by electron injection into the conduction band of the semiconductor host substrate,[18,42−49] with back electron transfer (involving recombination of the photooxidized surface complex with electrons in the conduction band) being several orders of magnitude slower than the forward electron-transfer reaction.[43,50−54] Such findings in high-surface area semiconductors led to the discovery of the low-cost, high-efficiency solar cell based on Ru-dye sensitization of colloidal TiO_2 films.[1] Presently, the most effective cells of this type are based on $Ru(dcbpy)_2(NCS)_2$ [dcvpy = (4,4′-dicarboxy-2,2′-bipyridine)] (RuN3)-sensitized nanocrystalline TiO_2 thin films.[1,9]

The ultrafast interfacial electron injection rates are commonly attributed to strong electronic couplings between states in the molecular adsorbates and the manifold of states in the semiconductor conduction band. This is in contrast to electron-transfer reactions in homogeneous solutions where the reactions rates are determined by the time scales for reorganization of nuclear coordinates. In addition, the much longer time scales associated with back electron-transfer processes, ranging from picosecond[18,43,45,46,50,51] to millisecond time scales[52,54,55] are likely due to trapping/detrapping dynamics of the injected electrons in the semiconductor NPs.[56,57] Notably, stabilization of coordination complexes by efficient surface-charge separation is not limited to Ru−polypyridyl complexes. The electronic couplings, responsible for ultrafast electron injection, are mainly determined by the nature of the molecular linkers,[58] and the recombination kinetics depends mainly on the distribution of trapping sites in the semiconductor NPs.[50]

Considering the nature of the underlying charge-separation dynamics at sensitized semiconductor interfaces, it is natural to expect that many other coordination compounds besides Ru−polypyridyl complexes could be photostabilized by attachment to semiconductor surfaces, including complexes prepared in high oxidation states generated by photoexcitation and IET. In fact, IET from coordination compounds of Rh, Re, Zn, Os, Ga, and Pt have already been investigated,[9,20−24] including a variety of molecular adsorbates such as chlorophyll derivatives,[59−62] porphyrins,[20,60,61,63] phthalocyanines,[64−71] platinum complexes,[72−74] coumarin 343,[75,76] and carboxylated derivatives of anthracene,[77,78] among others.[79−84] Surprisingly, Mn complexes have remained largely unexplored within the context of photoelectrochemical applications based on IET at semiconductor interfaces. Considering that Mn(III) is a strong oxidant, however, such a possibility will depend on the relative time scales for interfacial electron injection as compared to recombination dynamics.

Manganese coordination complexes have been extensively investigated as effective homogeneous catalysts for oxidation chemistry,[25−36] including biomimetic oxomanganese complexes based on terpyridine ligands that can be tuned for water splitting,[85] or regio- and stereoselective alkane hydroxylation.[86] The activation of these catalysts typically requires sacrificial

* To whom correspondence should be addressed. E-mail addresses: charles.schmuttenmaer@yale.edu; robert.crabtree@yale.edu; gary.brudvig@yale.edu; victor.batista@yale.edu.

10.1021/jp072380h CCC: $37.00
Published on Web 07/21/2007

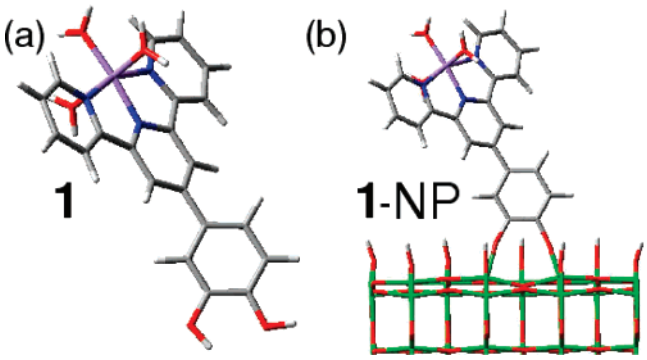

Figure 1. (a) Mn complex **1**: $[Mn^{II}(H_2O)_3(catechol\text{-}terpy)]^{2+}$ (terpy = 2,2′:6,2″-terpyridine); (b) surface-complex **1**/TiO_2−NP. Color scheme: C (gray), H (white), Mn (purple), N (blue), O (red), Ti (green).

electron scavengers (e.g., oxone or H_2O_2) that oxidize Mn to a sufficiently high valent state to enable it to react with H_2O, or aliphatic hydrocarbons, to form oxidized products such as O_2, alcohols, and epoxides.

This paper addresses the nontrivial question as to whether the oxidation state of Mn complexes can be advanced by photoexcitation and IET into semiconductor TiO_2 NPs, bypassing the need of consuming any primary oxidant and also avoiding production of the associated waste materials. The study is focused on the characterization of photoinduced IET between complex **(1)** $[Mn^{II}(H_2O)_3(catechol\text{-}terpy)]^{2+}$ (terpy = 2,2′:6,2″-terpyridine) and TiO_2 nanoparticles (see Figure 1). The time scale for Mn(II) → Mn(III) photooxidation due to ultrafast IET is determined by terahertz (THz) spectroscopy and computational modeling of the underlying interfacial quantum dynamics. The regeneration of the Mn(II) complex is monitored by time-resolved measurements of the Mn(II) EPR signal. The reported measurements and computational modeling show that functionalization of colloidal TiO_2 NPs can, indeed, be effectively used to activate a Mn(II) complex by photoexcitation and IET. Considering that Mn(III) complexes are effective catalysts for a wide range of oxidation reactions,[28−36] the reported results are expected to be particularly relevant to photocatalytic applications.

Experimental Procedures

Experimental results include UV/vis, time-resolved THz spectroscopy (TRTS), and electron paramagnetic resonance (EPR) of bare and sensitized TiO_2-anatase nanoparticles (NPs). Sample preparation and experimental procedures are described below. All reagents not specifically mentioned are purchased from Aldrich and used without further purification.

1. Preparation of TiO_2 NPs. Colloidal solutions containing nanoparticulate TiO_2 are prepared through hydrolysis of titanium tetraisopropoxide by following published procedures.[87] For a 500 mg/L solution, 500 mg of $Ti(OCH\text{-}(CH_3)_2)_4$ was dissolved in 20 mL of 2-propanol. A 2 mL aliquot of this solution was slowly injected (microsyringe) into 20 mL of water at pH = 1.5 (adjusted with HCl). The solution was clear since TiO_2 does not absorb in the visible spectrum; UV/vis measurements presented in the Results section show a sharp absorption band beginning at 380 nm, corresponding to a band gap of approximately 3.2 eV.

2. Preparation of the Catechol-Terpyridine Ligand 4′-(3,4-Dihydroxyphenyl)-2,2′:6′,2″-terpy. Catechol is used as obtained from Aldrich. The catechol-terpy ligand is synthesized according to published procedures.[88] A solution of 4′-(3,4-dimethoxyphenyl)-2,2′:6′,2″-terpyridine[89] (500 mg, 1.36 mmol) in HBr (25 mL) is refluxed for 5 h under nitrogen. The solution is allowed to cool to room temperature and then neutralized by addition of sodium bicarbonate. At neutral pH, the product precipitates and is collected by filtration and washed with distilled water. The solid product is then recrystallized from methanol as a yellow solid (245 mg, 53% yield). Anal. C, 69.67%; H, 4.69%; N, 11.43%. Calcs. for $C_{21}H_{15}N_3O_2\cdot H_2O$: C, 70.18%; H, 4.77%; N, 11.69%.

3. Sensitization of Suspended TiO_2 NPs with Catechol-Terpy and Catechol. UV−vis samples of catechol-TiO_2 and catechol-terpy-TiO_2 functionalized nanoparticles were made by dissolving either catechol (4.4 mg, 0.4 mmol) or catechol-terpy (13.6 mg, 0.4 mmol) in 2 mL of the colloidal suspensions of TiO_2 NPs. Stability of the catechol anchor to the TiO_2 surface in the presence of oxidizing compounds was established by exposing the sensitized NP films to peroxysulfate (oxone). The oxidant did not release the ligand over tens of minutes.

4. Preparation of Mesoporous Thin Films of Sensitized TiO_2 NPs. The samples for time-resolved terahertz and UV−vis spectroscopic measurements consist of thin mesoporous films (∼10 μm thick) of Degussa P25 TiO_2 nanoparticles. The nanoparticles were doctor bladed from aqueous solution onto a glass cover slip and annealed at 360 °C for 30 min. Degussa P25 consists of 25 nm particles that are 70% anatase and 30% rutile. The TiO_2 thin films are sensitized by soaking them overnight in 2 mM aqueous solution of catechol-terpy, or catechol. Mesoporous TiO_2 thin films sensitized with **1** are prepared by rinsing a catechol-terpy-sensitized film with distilled water and then soaking it in a 2 mM aqueous solution.

5. UV/vis Measurements. UV−visible absorbance spectra of bare and sensitized TiO_2 NPs in colloidal suspensions were done using 20 mM aqueous solutions of NPs at pH 1.5. The ∼10 nm particles did not scatter light, and measurements were done in transmission geometry. Films of P25 nanoparticles were highly scattering and spectra were obtained with a Varian Cary 3 spectrophotometer in diffuse transmission geometry using an integrating sphere. Reported spectra of nanoparticle films were taken using a dry NP film on a glass coverslip. Films covered with a drop of pH-neutral deionized water and then with a second coverslip, as used in THz measurements, were also measured and show similar behavior.

6. Time-Resolved Terahertz Spectroscopy Measurements. The experimental system for time-resolved terahertz spectroscopic measurements is depicted in Figure 2. An amplified Ti:sapphire laser (Tsunami/Spitfire from Spectra Physics) is used to generate 800 mW of pulsed near-IR light at 1 kHz. The pulse width is ∼100 fs and the center wavelength is 820 nm. About 2/3 of the power is frequency doubled and then filtered to produce 50 mW of 410 nm (3.02 eV) light for the pump beam. The remainder of the near-IR light is used to generate and detect terahertz radiation using a 4-parabola arrangement that focuses the THz to a spot size of ∼3 mm at the sample. Terahertz radiation is generated using optical rectification in a ZnTe crystal and detected using free space electro-optic sampling in a second ZnTe crystal. Terahertz data were taken at room temperature with the sample constantly moving to avoid photobleaching. The average of three samples was taken in each case. More details on the spectrometer and technique have been published previously.[90,91] Terahertz radiation is absorbed by mobile electrons in the TiO_2 conduction band and is insensitive to electrons within the adsorbed sensitizer. A decrease in broadband terahertz (0.2−2 THz) transmission in photoexcited samples

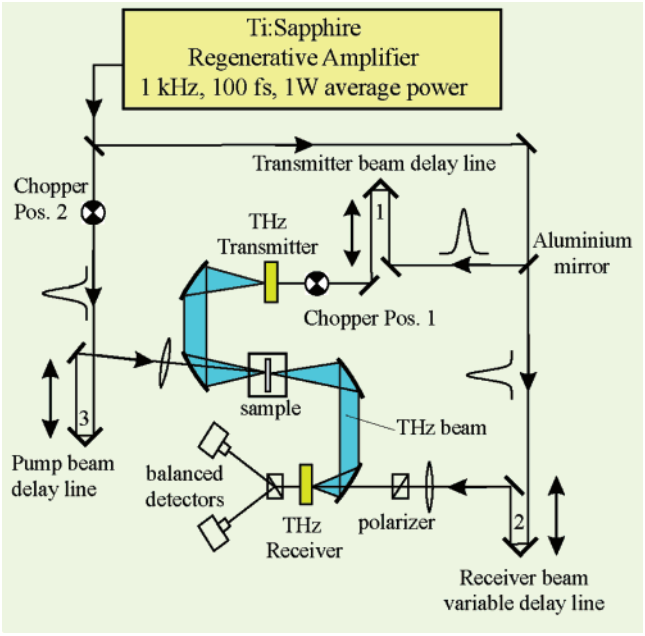

Figure 2. Experimental system for time-resolved THz spectroscopic measurements.

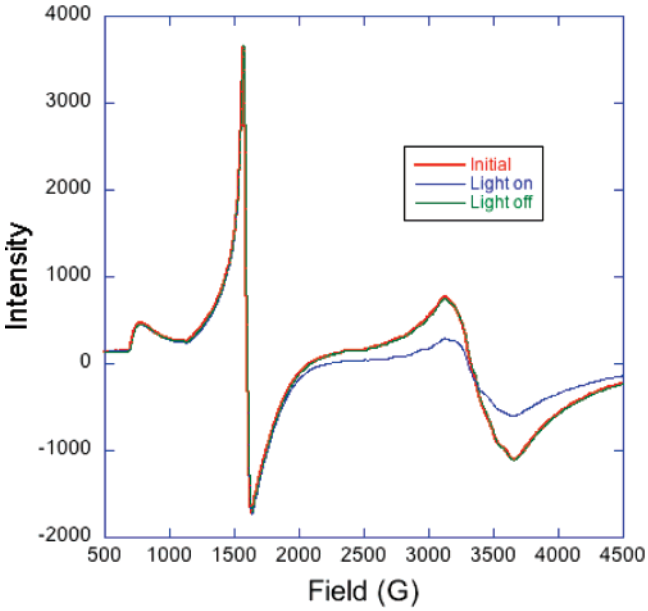

Figure 3. EPR spectra of TiO_2 NPs treated with catechol-terpy ligand functionalized with $Mn^{II}(OAc)_2$. The large signal at 1500 G is attributed to rhombic Fe^{III} impurities in the NPs. The iron signal was used as an internal standard to check for heating effects due to light absorption and to normalize by TiO_2 volume.

compared to nonphotoexcited samples indicates a higher electron density in the TiO_2. Injection time is measured by monitoring the change in terahertz transmission as the delay time between the 410 nm pump and the terahertz probe is varied.

7. EPR Spectroscopy. Perpendicular-mode EPR data were collected on an X-band Bruker Biospin/ELEXSYS E500 spectrometer equipped with a SHQ cavity and an Oxford ESR-900 liquid helium cryostat. All spectra were collected at 6 K on powdered samples sealed in capillary tubes placed in 5 mm OD quartz EPR tubes containing 60/40 toluene/acetone which forms a transparent glass for efficient illumination of the sample and allows efficient heat transfer to prevent heating of the sample during illumination (see Figure 3). All spectra were recorded with the following settings: modulation amplitude = 20 G, modulation frequency = 100 kHz, microwave power = 0.5 mW, and microwave frequency = 9.3863 GHz. Time course measurements follow the signal intensity at 3106 G. All illuminations were carried out in the cryostat with white light passed through 420 nm long-pass and water filters. Relative Mn^{II} concentrations are based on comparison of peak-to-peak amplitudes of both initial and illuminated signals at 3147 and 3674 G.

Computational Procedures

The simulations of UV−visible spectra are based on electronic structure calculations of TiO_2-anatase NP and NPs sensitized with catechol-terpy and catechol adsorbates. Simulations of electron injection include quantum-dynamics simulations of IET in TiO_2 NPs sensitized with catechol, catechol-terpy, and Mn complex **1**, which is a precursor of the mixed-valent di-μ-oxo-bridged manganese dimer $[Mn^{III}Mn^{IV}(\mu\text{-}O)_2(H_2O)_2(terpy)_2]^{3+}$.[92] Both sets of calculations are based on fully atomistic models of sensitized TiO_2-anatase NPs, as described by relaxed configurations optimized at the DFT level, in conjunction with a tight-binding model Hamiltonian gained from the extended-Hückel (EH) semiempirical approach[93] for electronic structure calculations as implemented in previous theoretical studies of sensitized TiO_2 NPs.[94] The EH method has been extensively implemented in calculations of the electronic structure of periodic systems. It requires a relatively small number of transferable parameters and is capable of providing semiquantitative descriptions of energy bands of elemental materials (including transition metals) as well as compound bulk materials in various phases.[95] The EH method is applicable to large extended systems and, contrary to plane-wave basis set approaches, provides valuable qualitative insight on the role of chemical bonding.[96] The method is, therefore, most suitable to develop a clear chemical picture of the nature of electronic transitions and the IET mechanism in sensitized TiO_2 NPs.

1. Catechol-Anatase Structure. Surface reconstruction due to TiO_2 functionalization with a catechol linker is described by geometry relaxation of extended supercells under vacuum conditions. Supercells are composed of catecholate molecules ($C_6H_4O_2$) adsorbed on the (101) surface of the TiO_2-anatase semiconductor ($32[TiO_2]$).[94] As depicted in Figure 4, the dimensions of the nanostructure are $1.0 \times 1.5 \times 3.1$ nm along the [-101], [010], and [101] directions, respectively. Periodic boundary conditions are imposed with a vacuum spacer between slabs, making negligible the interaction between distinct surfaces in the infinitely periodic model system. The surface dangling bonds are saturated with capping protons, in order to mimic acidic conditions, quenching the formation of surface states[97] and avoiding unphysical low coordination numbers. The DFT geometry relaxation is performed by using the Vienna Ab initio Simulation Package (VASP/VAMP)[98−100] implementing the PW91/GGA[101] approximation in a plane-wave basis ultrasoft Vanderbilt pseudopotentials[102] to describe the ionic interactions. The resulting structural relaxation next to the adsorbate describes the underlying surface reconstruction,[103] a process that is partially responsible for quenching the formation of surface states deep within the semiconductor band gap.[97]

2. Structure of the Surface Complex. The relaxed structure of catechol-terpy and complex **1** (shown in Figure 1a) are obtained through DFT minimum-energy geometry optimizations at the B3LYP/6-31G(d,p) level. Structures for catechol-terpy including coordination of the catecholate group to a hydrated Ti^{4+} ion were also obtained in analogy with previously published procedures.[104] All ab initio computations were performed using

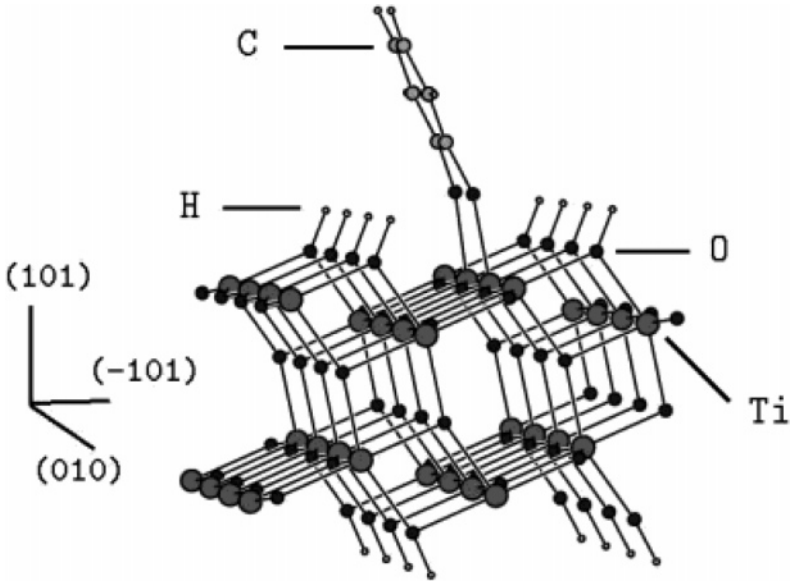

Figure 4. Unrelaxed configuration of the TiO_2-anatase model nanostructure sensitized with catechol, anchored on the (101) surface of the crystal under vacuum conditions. Large gray spheres represent Ti^{4+} ions, black spheres are O^{2-} ions, medium light-gray spheres are C atoms, and small light spheres are H atoms.

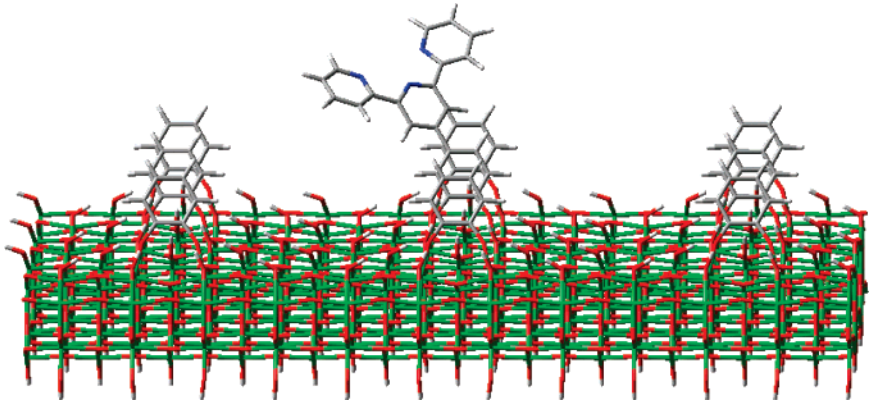

Figure 5. Supercell model of sensitized TiO_2 for simulations of IET.

the programs Jaguar 5.5[105] and Gaussian 03.[106] These calculations determine the relative orientation of the terpy and catechol groups; this information is then used in conjunction with the DFT-optimized catechol-anatase structure obtained as described above to determine the full surface complex structure (as depicted for example in Figure 1b.

3. Electronic Structure. The EH electronic Hamiltonian used for the calculation of the UV/visible spectra of the bare and sensitized nanoparticles and the simulations of electron injection allows a clear chemical picture of the IET mechanism in terms of transient populations of specific electronic states, at the semiquantitative level. The EH Hamiltonian is computed in the basis of Slater-type orbitals for the radial part of the atomic orbital (AO) wavefunctions.[93] The basis set includes the 3d, 4s, and 4p atomic orbitals of Ti^{4+} and Mn^{2+}; the 2s and 2p orbitals of O^{2-}, N, and C; and the 1s orbitals of H. This amounts to a set of 596 basis functions for the representation of the Hamiltonian matrix associated with the nanostructure shown in Figure 4. Simulations of electron injection were conducted in extended models constructed by the juxtaposition of heterogeneous supercells (e.g., see Figure 5). These extended models are necessary since simulations of charge injection in smaller clusters (e.g., 1.2 nm nanostructures without periodic boundary conditions) would be affected by surface states that speed up the electron-injection process while the implementation of periodic boundary conditions may introduce artificial recurrences (i.e., artificial back-electron-transfer events).[94]

4. Simulations of UV/Visible Spectra. The EH Hamiltonian of the bare and functionalized NPs is diagonalized in the basis of AOs by solving the generalized EH eigenvalue problem, $HQ^q = E_qSQ^q$, where H is the EH matrix, S is the atomic orbital overlap matrix, and Q^q are the expansion coefficients of the molecular orbital (MO) with eigenvalue E_q. Then, the oscillator strength f of the transition with energy $E_{q'} - E_q$ is computed by the expression $f \approx 8\pi^2\bar{\nu}cm/(3he^2)|\langle\psi_{q'}|e\bar{r}|\psi_q\rangle|^2$, where $\bar{r}$ is the electron position operator, $\bar{\nu}$ is the wavenumber of the transition, c is the speed of light, m is the electron mass, h is Planck's constant, and $|\psi_q\rangle$ is the position space wavefunction of the MO with eigenvalue E_q.[93]

The resulting spectra are obtained by convolution of each set of discrete transitions with a Gaussian function (fwhm = 67 nm) to match the experimental resolution function. The oscillator strengths are used to assign relative weights to the transitions and the total absorbance is globally scaled to facilitate the comparison with the experimental results. The diagonalized Hamiltonians correspond to structures analogous to that shown in Figure 4, with and without the catechol as well as with the terpy attached to the adsorbed catechol. Further investigation into the nature of these electronic transitions has been accomplished by simulating the UV/vis spectra of the catechol-

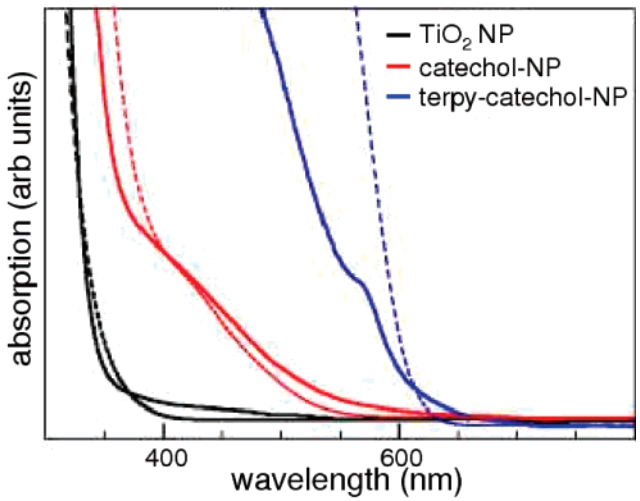

Figure 6. Experimental (solid lines) and theoretical (dashed lines) UV−visible spectra of colloidal suspensions of bare TiO_2 NPs (black) and TiO_2 NPs functionalized with catechol (red) and terpyridine-catechol (blue).

terpy-Ti(OH)$_4$ subsystem at the TDDFT/B3LYP/6-31G(d,p) level, showing strong intraligand excitations in the visible-UV region.

5. Simulations of IET. Computations of the survival probability, $\rho_{MOL}(t)$ allow the characterization of the IET time scales. $\rho_{MOL}(t)$ is defined as the probability that at time t, after excitation of the system, the photoexcited electron is still in the adsorbate molecule.[94] It is computed as the projection of the time-evolved electronic wave function onto the AOs of the molecular adsorbate.

The time-evolved wave function is written as a linear combination of AOs $|\Psi(t)\rangle = \sum_i B_i(t)|\chi_i\rangle$ where the $|\chi_i\rangle$ represent the atomic orbitals. The expansion coefficients $B_i(t)$ are computed according to $B_i(t) = \sum_q Q_i^q C_q \exp[-(i/\hbar)E_q t]$, where the vectors Q^q are described as in the previous section and the C_q are defined by the expansion of the initial state in the orthonormal basis ket sets $|\Psi(0)\rangle = \sum_q C_q|q\rangle$.

The survival probability is computed as $\rho_{MOL}(t) = |\sum_i^{MOL}\sum_j B_i^*(t)B_j(t)S^{ij}|$ where S is the atomic orbital overlap matrix introduced above. To avoid artificial recurrences in electron-transient populations, the calculations of charge injection are conducted in models consisting of nine juxtaposed catechol-anatase blocks, with the center block containing the larger surface complex (see Figure 5). Initial states for the various simulations are determined assuming instantaneous photoexcitation of the surface complex by allowed transitions in the visible region.

Results

1. Visible-Light Sensitization. Figure 6 shows the comparison of experimental (solid lines) and theoretical (broken lines) UV−visible absorption spectra of bare TiO_2 anatase NPs and NPs functionalized by catechol and catechol-terpy adsorbates. Experimental UV−vis spectra correspond to 20 mM aqueous suspensions of TiO_2 NPs at pH = 1.5. Theoretical spectra are obtained by computing cumulative transition dipole moments between discrete energy levels of functionalized TiO_2 NPs, as described by a tight-binding model Hamiltonian.[94] To facilitate the comparison with experimental data, the resulting spectrum is convoluted with the experimental resolution function.

The spectra of the bare TiO_2 NPs and catechol/TiO_2 NPs serve as spectroscopic benchmarks, comparing well with results in the literature.[107] In particular, the spectrum of anatase TiO_2 shows the characteristic absorption edge at $\lambda \approx 380$ nm due to electronic transitions between the valence and the conduction bands. In contrast, surface functionalization with catechol gives rise to a superimposed broad shoulder with a long tail, extending beyond $\lambda \approx 600$ nm. The resulting shoulder absorption band, centered at $\lambda \approx 425$ nm, can be assigned to direct electronic transitions between the ligand and the TiO_2 conduction band.[108,109] Sensitization of TiO_2 NPs with the catechol-terpyridine ligand leads to a pronounced red shift in the photoabsorption spectrum, shifting the absorption edge to about $\lambda \approx 650$ nm.

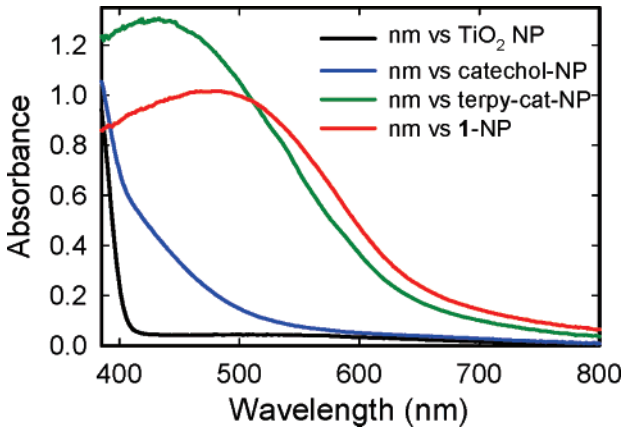

Figure 7. Experimental UV−visible spectra of films of bare TiO_2 NP (black), and films of TiO_2 NPs functionalized with catechol (blue), terpyridine-catechol (green) and Mn(II)-terpyridine-catechol (red).

UV−vis absorption spectra were also measured for the NP films used for electron injection measurements, Figure 7. NP films are made from ~25 nm P25 nanoparticles which are 70% anatase and 30% rutile instead of the 5−10 nm anatase nanoparticles used for the suspended nanoparticle UV−vis measurements. The films are highly scattering, so measurements were taken in diffuse transmission geometry. The NP films show absorbance onsets at wavelengths similar to those of the aqueous suspensions of NPs. The absorption onset of the bare TiO_2 NP films is slightly red-shifted compared to the suspension's because of the presence of rutile (E_g = 3.01 eV). Adsorption of catechol results in a shoulder centered at ~425 nm with a long tail extending to over 550 nm. Terpy-catechol-NP shows strong absorbance beginning at ~600 nm with a peak at 425 nm. The onset red-shifts further still with **1**-NP, which exhibits a peak at 475 nm. The crossover of **1**-NP with the other three spectra results from its slightly smaller film thickness. Adsorption of complex **1** sensitizes TiO_2 over the entire visible spectrum.

The molecular origin of the red-shifted photoabsorption band for the catechol-terpyridine-NP and **1**-NP can be assigned to direct transitions between the ligand and the TiO_2 conduction band as well as to electronic excitations within the surface complex. These include transitions from states significantly overlapping the catechol-HOMO to states of the conduction band, as well as to states localized in the surface complex. These results demonstrate visible sensitization of TiO_2 thin films by surface functionalization with Mn complexes. The quantum mechanical analysis of the density of states indicates that such an electron-donor state is energetically localized at about 1.5 eV below the Fermi level of **1**-NP and that the Fermi level corresponds to an electronic state localized on Mn. This suggests that spontaneous internal conversion after photoexcitation and IET could oxidize Mn(II) in the surface complex.

2. Ultrafast Interfacial Electron Transfer. Figure 8a shows ultrafast interfacial electron injection induced by 410 nm

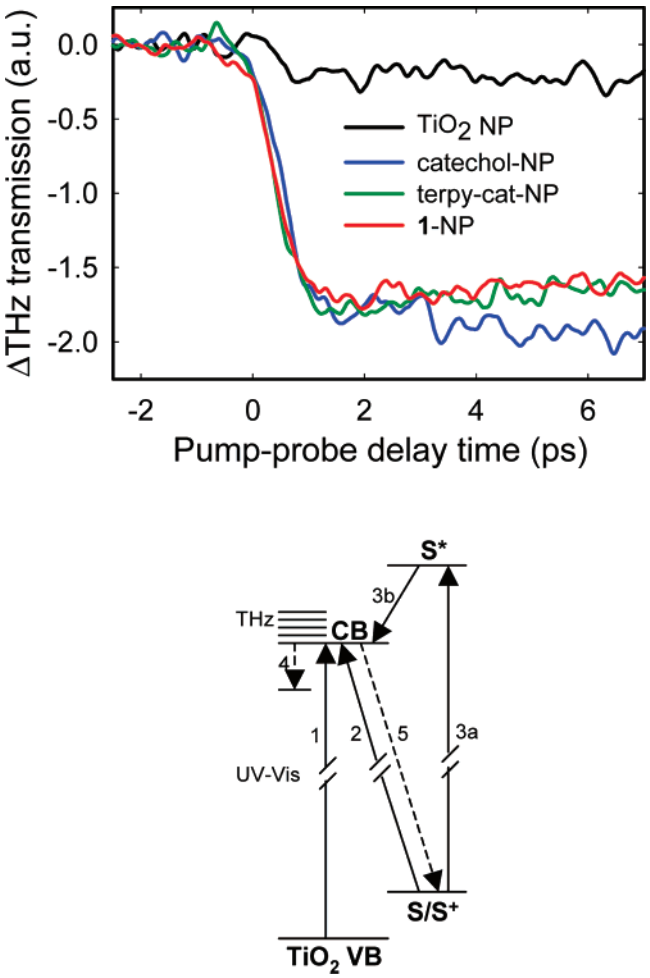

Figure 8. (a) 410 nm pump/THz probe of electron injection in functionalized TiO_2 NP films. (b) Schematic of possible electron injection pathways into TiO2 from bulk photoexcitation (1) or from photoexcitation of the sensitizer, S/S*, (2 and 3). Electrons can also become trapped in TiO2 (4) and recombine with the oxidized sensitizer (5). 1−3 cause a decrease in THz transmission, whereas 4 and 5 cause an increase.

photoexcitation of TiO_2 NP colloidal thin films, including bare TiO_2 and TiO_2 NP's functionalized with catechol, catechol-terpy, and Mn(II)-terpy-catechol (**1**) adsorbates. The noncontact THz probe allows for the comparative analysis of charge injection efficiency and time scale in bare and functionalized TiO_2 NPs with subpicosecond resolution,[110] since THz radiation is absorbed by free electrons in the TiO_2 conduction band. Photoexcitation and subsequent electron injection causes the free carrier population in the TiO_2 to increase, resulting in a decrease in THz transmission.

Since the photoexcitation energy of the pump−pulse is near the band edge of the TiO_2, there are three possible pathways for electrons to be injected into the TiO_2 conduction band as shown in Figure 8b. They are as follows: (1) direct photoexcitation of bulk TiO_2 ,(2) direct transitions from the sensitizer into the TiO_2 conduction band, and (3) photoexcitation of the sensitizer, followed by relaxation to the TiO_2 conduction band. Direct injection from catechol into Ti 3d states has previously been experimentally observed.[109] In cases 2 and 3, the sensitizer could inject from orbitals localized on the catechol part of the sensitizer or from orbitals localized to the terpy-Mn. All of these are viable pathways to the creation of Mn(III) since injection from catechol orbitals could be followed by catechol reduction by Mn(II).

Figure 8a shows an 8-fold enhancement in THz absorbance for the sensitized versus the non-sensitized NP films, confirming charge injection from the photoexcited sensitizer via pathways 2 and/or 3. The magnitudes of the changes in terahertz transmission through NP films sensitized with each of the three adsorbates are essentially the same. Although the transmission unit in Figure 8a is arbitrary, the same scaling factor is used for all samples so amplitude comparisons are meaningful, i.e., no normalization has been performed. In the thin film, low absorbance limit, one would expect that the relative signal sizes of the different sensitizers would be related to their UV−vis absorbance shown in Figure 7 and to the quantum efficiency of the injection process. However, since the TiO_2 films were thicker than the optical skin depth of the 410 nm pump for each adsorbate, the photon flux limits the signal size. Although the less absorbing catechol-NP is expected to have a lower concentration of injected electrons spread throughout a larger depth than **1**-NP, the same total number of injected electrons are present to absorb the THz probe radiation. That all of the sensitized NPs showed similarly large signal indicates that 410 nm light is absorbed by states which are strongly coupled to the TiO_2, resulting in injection with high quantum efficiency. To the contrary, the bare TiO_2 film signal is limited by the low TiO_2 absorbance of 410 nm light. According to the UV−vis spectroscopy in Figure 7, ∼90% of 410 nm light is absorbed by sensizited NPs, whereas only ∼10% is absorbed by bare TiO_2.

The ultrafast spectroscopic data, Figure 8a, indicate that IET from the adsorbate to the NP is completed in the subpicosecond time scale after photoexcitation of the system. The time-resolved terahertz injection data are well fit using a single exponential with time constant of ∼300 fs convoluted with a Gaussian instrument response function for each of the sensitizers. The value of 300 fs actually represents an upper bound on the injection time scale, since this approaches the limit of the time resolution of ∼500 fs for the spectrometer. Additionally, THz radiation is only sensitive to mobile electrons. If injected electrons are initially bound at surface sites[111] or exhibit low mobility before thermalizing with the TiO_2 lattice,[112] they will be invisible or less visible to the THz probe.[90] The 300 fs would then correspond to the time for electrons to become highly mobile, while the time scale for interfacial electron injection is potentially much faster. THz measurements taken over hundreds of picoseconds do not show any slower injection components for any of the sensitizers. However, we cannot exclude the possibility that there are multiple timescales for injection from the various pathways mentioned previously but that all timescales are equal to or faster than our experimental resolution.

The THz absorbance signal decays exponentially with a half-life of ∼300 ps for each of the three sensitizers, indicating that the injected electrons have become trapped at TiO_2 defects or surface sites, or have recombined with either oxidized adsorbates or oxidants in the solution. However, the Mn(III) created by photo-oxidation of **1** could remain stable for much longer since the photogenerated electron and hole are no longer correlated. Previous experiments show recombination in sensitized NP systems to occur on timescales ranging from picoseconds to milliseconds,[113] and the lifetimes of the electron and of the Mn(III) are expected to depend strongly on the composition of the solution surrounding the NP film.

Figure 9 shows results of calculations of the time-dependent adsorbate populations, for representative nuclear trajectories relaxing after instantaneous visible excitation of catechol, catechol-terpy, and the Mn(II)-terpy-catechol complex **1**.

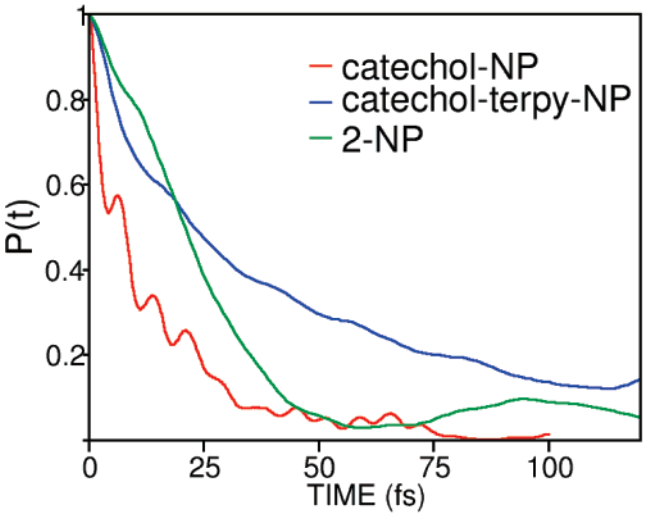

Figure 9. Computed survival probabilities corresponding to photoexcited surface complexes. Each curve represents the probability of the electron to remain in the respective photoexcited surface complex.

Time-dependent populations are obtained by solving the electronic time-dependent Schrödinger equation according to a mixed quantum-classical approach[94] and projecting the time-evolved electronic wave packet onto the atomic orbitals of the molecular adsorbate. These calculations predict that typical electron injection events are completed within 50−100 fs, a time scale that is shorter than the ∼500 fs instrument response function of our THz spectroscopic measurements.

Figure 10 shows a detailed analysis, at the molecular level, of the time-dependent charge distribution following instantaneous excitation of a **1**-NP surface complex. This particular simulation is for excitation from the LUMO+2 level of **1** and is a representative picture. In reality, several different states can be photoexcited followed by injection of electrons into TiO_2. Some will have the initial excitation more localized around catechol, whereas others would be more localized around the terpy ligand. The series of snapshots shown in Figure 10 indicates that the early time mechanism of IET involves depletion of electronic density localized in the catechol linker and electron injection into d_{xz} orbitals of Ti^{4+} ions, next to the surface complex. The subsequent relaxation mechanism involves charge diffusion and surface-charge separation. These results indicate the directional character of the relaxation dynamics where injection, rather than intraligand relaxation, is clearly the preferred relaxation pathway. Figure 10 also shows how an electron photoexcited to a π^* orbital of the catechol-terpyridine ligand, directly injects into the TiO_2 conduction band. Examining the mechanism of IET at this level of detail also supports earlier conclusions about the crucial role of π^* electronic states, associated with aromatic ligands, as important electronic gateways responsible for mediating ultrafast IET from TiO_2 surface complexes.[114,115]

3. Recombination Dynamics. Figure 11a shows EPR spectra of colloidal TiO_2 films functionalized with the Mn complex (**1**), before, during, and after illumination at 6 K. In the dark, the characteristic signal of Mn^{II} is clearly visible (black). After illumination with a broad-spectrum Xe lamp, fitted with a filter transmitting only $\lambda \geq 420$ nm, the Mn^{II} signal decays (red), indicating oxidation to Mn^{III}. After the lamp is blocked, the Mn^{II} signal is regenerated in the absence of electron scavengers (blue), indicating reversible photoinduced charge separation.

Figure 11b shows the time-dependent fraction of Mn(II) surface complexes, when turning the light on (↑) and off (↓) at 6 K. The loss of Mn(II) is faster than the EPR instrument response time and is consistent with the sub-ps injection time seen in the THz experiments. The 23 s time scale for e^-/h^+ recombination at 6 K is much longer than the 1 ms upper limit for carrier trapping and/or recombination time as measured at room temperature by the THz experiments (using a 1 kHz repetition rate laser, with no residual signal from the previous laser shot with detected). Room-temperature EPR was also performed, but no change in signal was detected upon illumination, indicating Mn(III) formation and reduction within EPR's 1 ms time resolution, again consistent with the THz measurements. It is known that e^-/h^+ recombination times are highly temperature dependent. Future EPR studies at higher temperatures, and THz studies at lower temperatures, will allow us to compare recombination times from both experiments.

Conclusions

We conclude that Mn complex **1**, $[Mn^{II}(H_2O)_3(catechol\text{-}terpy)]^{2+}/TiO_2$ (terpy = 2,2′:6,2″-terpyridine), photosensitizes TiO_2 NPs to visible light absorption. It exhibits efficient charge separation and reversible photochemistry when bound to TiO_2 NPs in colloidal thin films or aqueous suspensions, even in advanced oxidation states generated by photoexcitation and IET.

The simulations of IET into TiO_2 NPs sensitized with catechol, catechol-terpy, and Mn complex **1** are consistent with the THz measurements, providing a detailed molecular level description of a possible electron injection mechanism. Furthermore, there is good agreement between the calculated and measured steady-state UV/vis absorption spectra of the bare TiO_2 NPs, and those sensitized with catechol and catechol-terpy adsorbates, consistently predicting sensitization of TiO_2 NPs to visible-light.

In analogy to other sensitized TiO_2 materials, the observed stability of the Mn−surface complex is correlated to the highly efficient charge-separation processes triggered by photoexcitation, including photooxidation of the surface complex and

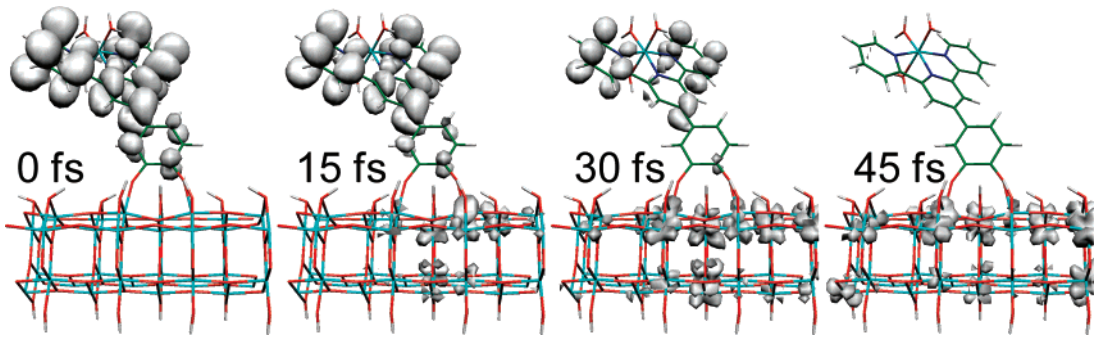

Figure 10. Snapshots of the electronic charge distribution, during the IET from the LUMO+2 of **1**. Only the local TiO_2 structure, next to photoexcited adsorbate is shown for detailed view of the time dependent charge distribution.

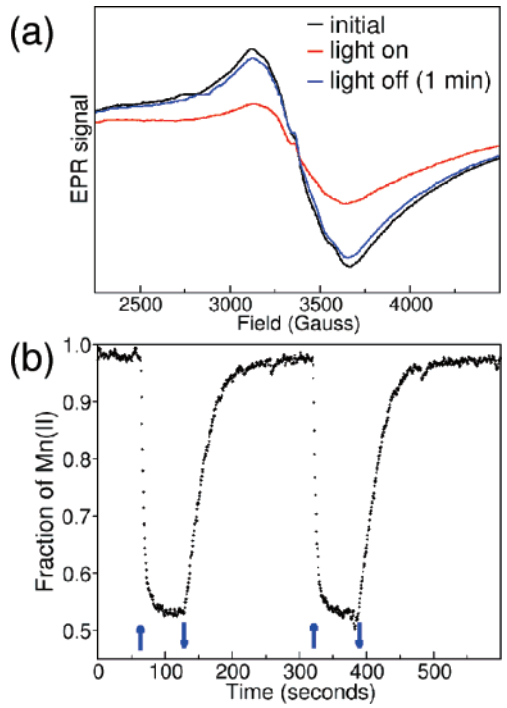

Figure 11. (a) EPR signal at 6 K characteristic of Mn(II): black/blue are dark adapted samples and red correspond to samples under visible light; (b) Time-dependent EPR signal when turning on (↑) and off (↓) the visible light irradiance.

ultrafast IET into the conduction band of TiO_2. Regeneration of the initial Mn complex by e^-/h^+ recombination is probably limited by the underlying trapping/detrapping dynamics of the photoinjected electrons within the TiO_2 NPs. The EPR studies show it to be on the order of 20 s at 6 K, and the THz experiments bracket it between 500 ps and 1 ms at room temperature.

Prolonged stability of the photooxidized Mn(III) surface complex would be ideally suited for photocatalytic applications, currently under study in our group. However, catalysis at 6 K to take advantage of ~20 s recombination times is clearly not feasible. On the other hand, even recombination times on the order of nanoseconds to hundreds of microseconds at room temperature, which are consistent with the present observations, would allow significant catalytic activity.

Acknowledgment. V.S.B. acknowledges supercomputer time from NERSC and financial support from Research Corporation RI0702, ACS PRF# 37789-G6, NSF CHE# 0345984, an Alfred P. Sloan Fellowship (2005-2007) and a Camille Dreyfus Teacher-Scholar Award. J.B.B. acknowledges the Donors of the ACS PRF for support via an Alternative Energy Postdoctoral Fellowship. C.A.S. acknowledges support from NSF CHE# 0616875 for partial support of this work. R.H.C. acknowledges NSF CHE-0614403 for support. G.W.B acknowledges support from NIH Grant GM32715. NSF Grant CHE-0215926 provided funds to purchase the ELEXSYS E500 EPR spectrometer. The authors thank Dr. Tijana Rajh, from Argonne National Laboratory, for providing colloidal TiO_2 NPs for the spectroscopic characterization of thin films.

References and Notes

(1) O'Regan, B.; Gratzel, M. *Nature* **1991**, *353*, 737.
(2) Nazeeruddin, M. K.; Kay, A.; Rodicio, I.; Humphrybaker, R.; Muller, E.; Liska, P.; Vlachopoulos, N.; Gratzel, M. *J. Am. Chem. Soc.* **1993**, *115*, 6382.
(3) Serpone, N. *Res. Chem. Interm.* **1994**, *20*, 953.
(4) Serpone, N.; Lawless, D.; Disdier, J.; Herrmann, J. M. *Langmuir* **1994**, *10*, 643.
(5) Serpone, N.; Terzian, R.; Hidaka, H.; Pelizzetti, E. *J. Phys. Chem.* **1994**, *98*, 2634.
(6) Mills, A.; LeHunte, S. *J. Photochem. Photobiol. A* **1997**, *108*, 1.
(7) Colvin, V. L.; Schlamp, M. C.; Alivisatos, A. P. *Nature* **1994**, *370*, 354.
(8) Furtado, L. F. O.; Alexiou, A. D. P.; Goncalves, L.; Toma, H. E.; Araki, K. *Ang. Chem.-Int. Ed.* **2006**, *45*, 3143.
(9) Nazeeruddin, M. K.; Kay, A.; Rodicio, I.; Humphrybaker, R.; Muller, E.; Liska, P.; Vlachopoulos, N.; Gratzel, M. *J. Am. Chem. Soc.* **1993**, *115*, 6382.
(10) Polo, A. S.; Itokazu, M. K.; Iha, N. Y. M. *Coord. Chem. Rev.* **2004**, *248*, 1343.
(11) Sheng, X. L.; Zhao, Y.; Zhai, J.; Zhu, D. B. *Prog. Chem.* **2007**, *19*, 59.
(12) Kim, K. E.; Jang, S. R.; Park, J.; Vittal, R.; Kim, K. J. *Sol. Ener. Mat. Sol. Cells* **2007**, *91*, 366.
(13) Reemts, J.; Kittel, A. *J. Appl. Phys.* **2007**, *101*.
(14) Roh, S. J.; Mane, R. S.; Min, S. K.; Lee, W. J.; Lokhande, C. D.; Han, S. H. *Appl. Phys. Lett.* **2006**, *89*.
(15) Mane, R. S.; Lee, W. J.; Pathan, H. M.; Han, S. H. *J. Phys. Chem. B* **2005**, *109*, 24254.
(16) Niinobe, D.; Makari, Y.; Kitamura, T.; Wada, Y.; Yanagida, S. *J. Phys. Chem. B* **2005**, *109*, 17892.
(17) Green, A. N. M.; Palomares, E.; Haque, S. A.; Kroon, J. M.; Durrant, J. R. *J. Phys. Chem. B* **2005**, *109*, 12525.
(18) Hao, E. C.; Anderson, N. A.; Asbury, J. B.; Lian, T. Q. *J. Phys. Chem. B* **2002**, *106*, 10191.
(19) Asbury, J. B.; Ellingson, R. J.; Ghosh, H. N.; Ferrere, S.; Nozik, A. J.; Lian, T. Q. *J. Phys. Chem. B* **1999**, *103*, 3110.
(20) Deng, H. H.; Zhou, Y. M.; Mao, H. F.; Lu, Z. H. *Synth. Met.* **1998**, *92*, 269.
(21) Heimer, T. A.; Darcangelis, S. T.; Farzad, F.; Stipkala, J. M.; Meyer, G. J. *Inorg. Chem.* **1996**, *35*, 5319.
(22) Campbell, W. M.; Burrell, A. K.; Officer, D. L.; Jolley, K. W. *Coord. Chem. Rev.* **2004**, *248*, 1363.
(23) Argazzi, R.; Iha, N. Y. M.; Zabri, H.; Odobel, F.; Bignozzi, C. A. *Coord. Chem. Rev.* **2004**, *248*, 1299.
(24) Kalyanasundaram, K.; Vlachopoulos, N.; Krishnan, V.; Monnier, A.; Gratzel, M. *J. Phys. Chem.* **1987**, *91*, 2342.
(25) Wessel, J.; Crabtree, R. H. *J. Mol. Cat. A-Chem.* **1996**, *113*, 13.
(26) Taft, K. L.; Kulawiec, R. J.; Sarneski, J. E.; Crabtree, R. H. *Tetrahedron Lett.* **1989**, *30*, 5689.
(27) Beck, W. F.; Sears, J.; Brudvig, G. W.; Kulawiec, R. J.; Crabtree, R. H. *Tetrahedron* **1989**, *45*, 4903.
(28) Choudary, B. M.; Pal, U.; Kantam, M. L.; Ranganath, K. V. S.; Sreedhar, B. *Adv. Synth. Catal.* **2006**, *348*, 1038.
(29) Bagherzadeh, M.; Latifi, R.; Tahsini, L. *J. Mol. Catal. A-Chem.* **2006**, *260*, 163.
(30) Collman, J. P.; Zeng, L.; Wang, H. J. H.; Lei, A.; Brauman, J. I. *Eur. J. Org. Chem.* **2006**, 2707.
(31) Silva, A. R.; Wilson, K.; Clark, J. H.; Freire, C. Asymmetric epoxidation of alkenes by a chiral manganese(III) salen complex anchored onto a functionalised hexagonal mesoporous silica. In *Molecular Sieves: From Basic Research to Industrial Applications, Pts a and B* **2005**, Vol. 158, pp 1525.
(32) Barroso, S.; Blay, G.; Fernandez, I.; Pedro, J. R.; Ruiz-Garcia, R.; Pardo, E.; Lloret, F.; Munoz, M. C. *J. Mol. Cat. A-Chem.* **2006**, *243*, 214.
(33) Cardoso, B.; Pires, J.; Carvalho, A. P.; Kuzniarska-Biernacka, I.; Silva, A. R.; de Castro, B.; Freire, C. *Microporous Mesoporous Mater.* **2005**, *86*, 295.
(34) Nunes, G. S.; Mayer, I.; Toma, H. E.; Araki, K. *J. Catal.* **2005**, *236*, 55.
(35) Borriello, C.; Del, Litto, R.; Panunzi, A.; Ruffo, F. *Inorg. Chem. Comm.* **2005**, *8*, 717.
(36) Rebelo, S. L. H.; Simoes, M. M. Q.; Neves, M.; Silva, A. M. S.; Tagliatesta, P.; Cavaleiro, J. A. S. *J. Mol. Catal. A* **2005**, *232*, 135.
(37) Connolly, J. S. *Photochemical conversion and storage of solar energy*; Academic Press: New York, 1981.
(38) Gratzel, M. *Energy resources through photochemistry and catalysis*; Academic Press: New York, 1983.
(39) Wrighton, M. S. *J. Chem. Edu.* **1983**, *60*, 877.
(40) Gratzel, M. *Coord. Chem. Rev.* **1991**, *111*, 167.
(41) Bard, A. J.; Fox, M. A. *Acc. Chem. Res.* **1995**, *28*, 141.
(42) Heimer, T. A.; Heilweil, E. J.; Bignozzi, C. A.; Meyer, G. J. *J. Phys. Chem. A* **2000**, *104*, 4256.
(43) Ghosh, H. N.; Asbury, J. B.; Weng, Y. X.; Lian, T. Q. *J. Phys. Chem. B* **1998**, *102*, 10208.
(44) Cherepy, N. J.; Smestad, G. P.; Gratzel, M.; Zhang, J. Z. *J. Phys. Chem. B* **1997**, *101*, 9342.
(45) Martini, I.; Hodak, J.; Hartland, G. V.; Kamat, P. V. *J. Chem. Phys.* **1997**, *107*, 8064.

(46) Martini, I.; Hodak, J. H.; Hartland, G. V. *J. Phys. Chem. B* **1998**, *102*, 9508.
(47) Tachibana, Y.; Moser, J. E.; Gratzel, M.; Klug, D. R.; Durrant, J. R. *J. Phys. Chem.* **1996**, *100*, 20056.
(48) Hannappel, T.; Burfeindt, B.; Storck, W.; Willig, F. *J. Phys. Chem. B* **1997**, *101*, 6799.
(49) Ellingson, R. J.; Asbury, J. B.; Ferrere, S.; Ghosh, H. N.; Sprague, J. R.; Lian, T. Q.; Nozik, A. J. *J. Phys. Chem. B* **1998**, *102*, 6455.
(50) Weng, Y. X.; Wang, Y. Q.; Asbury, J. B.; Ghosh, H. N.; Lian, T. Q. *J. Phys. Chem. B* **2000**, *104*, 93.
(51) Martini, I.; Hodak, J. H.; Hartland, G. V. *J. Phys. Chem. B* **1999**, *103*, 9104.
(52) Lu, H.; Prieskorn, J. N.; Hupp, J. T. *J. Am. Chem. Soc.* **1993**, *115*, 4927.
(53) Weng, Y. X.; Wang, Y. Q.; Asbury, J. B.; Ghosh, H. N.; Lian, T. Q. *J. Phys. Chem. B* **2000**, *104*, 93.
(54) Vrachnou, E.; Vlachopoulos, N.; Gratzel, M. *J. Chem. Soc.* **1987**, 868.
(55) Blackbourn, R. L.; Johnson, C. S.; Hupp, J. T. *J. Am. Chem. Soc.* **1991**, *113*, 1060.
(56) Nelson, J. *Phys. Rev. B* **1999**, *59*, 15374.
(57) Barzykin, A. V.; Seki, K.; Tachiya, M. *J. Phys. Chem. B* **1999**, *103*, 9156.
(58) Galoppini, E. *Coord. Chem. Rev.* **2004**, *248*, 1283.
(59) Kay, A.; Humphrybaker, R.; Gratzel, M. *J. Phys. Chem.* **1994**, *98*, 952.
(60) Kay, A.; Gratzel, M. *J. Phys. Chem.* **1993**, *97*, 6272.
(61) Kamat, P. V.; Chauvet, J. P.; Fessenden, R. W. *J. Phys. Chem.* **1986**, *90*, 1389.
(62) Bedja, I.; Hotchandani, S.; Carpentier, R.; Fessenden, R. W.; Kamat, P. V. *J. Appl. Phys.* **1994**, *75*, 5444.
(63) Kalyanasundaram, K.; Vlachopoulos, N.; Krishnan, V.; Monnier, A.; Gratzel, M. *J. Phys. Chem.* **1987**, *91*, 2342.
(64) Fan, F. R. F.; Bard, A. J. *J. Am. Chem. Soc.* **1979**, *101*, 6139.
(65) Giraudeau, A.; Fan, F. R. F.; Bard, A. J. *J. Am. Chem. Soc.* **1980**, *102*, 5137.
(66) Hodak, J.; Quinteros, C.; Litter, M. I.; Roman, E. S. *J. Chem. Soc.-Faraday Trans.* **1996**, *92*, 5081.
(67) Fang, J. H.; Wu, J. W.; Lu, X. M.; Shen, Y. C.; Lu, Z. H. *Chem. Phys. Lett.* **1997**, *270*, 145.
(68) Nazeeruddin, M. K.; Humphry-Baker, R.; Gratzel, M.; Murrer, B. A. *Chem. Commun.* **1998**, 719.
(69) Nazeeruddin, M. K.; Humphry-Baker, R.; Gratzel, M.; Wohrle, D.; Schnurpfeil, G.; Schneider, G.; Hirth, A.; Trombach, N. *J. Porphyrins Phthalocyanines* **1999**, *3*, 230.
(70) He, J. J.; Hagfeldt, A.; Lindquist, S. E.; Grennberg, H.; Korodi, F.; Sun, L. C.; Akermark, B. *Langmuir* **2001**, *17*, 2743.
(71) Aranyos, V.; Hjelm, J.; Hagfeldt, A.; Grennberg, H. *J. Porphyrins Phthalocyanines* **2001**, *5*, 609.
(72) Paw, W.; Cummings, S. D.; Mansour, M. A.; Connick, W. B.; Geiger, D. K.; Eisenberg, R. *Coord. Chem. Rev.* **1998**, *171*, 125.
(73) Islam, A.; Sugihara, I.; Hara, I.; Singh, L. P.; Katoh, R.; Yanagida, M.; Takahashi, Y.; Murata, S.; Arakawa, H. *New J. Chem.* **2000**, *24*, 343.
(74) Islam, A.; Sugihara, H.; Hara, K.; Singh, L. P.; Katoh, R.; Yanagida, M.; Takahashi, Y.; Murata, S.; Arakawa, H. *Inorg. Chem.* **2001**, *40*, 5371.
(75) Enea, O.; Moser, J.; Gratzel, M. *J. Electroanal. Chem.* **1989**, *259*, 59.
(76) Rehm, J. M.; McLendon, G. L.; Nagasawa, Y.; Yoshihara, K.; Moser, J.; Gratzel, M. *J. Phys. Chem.* **1996**, *100*, 9577.
(77) Kamat, P. V.; Ford, W. E. *Chem. Phys. Lett.* **1987**, *135*, 421.
(78) Kamat, P. V. *J. Phys. Chem.* **1989**, *93*, 859.
(79) Moser, J.; Gratzel, M. *J. Am. Chem. Soc.* **1984**, *106*, 6557.
(80) Vrachnou, E.; Gratzel, M.; McEvoy, A. J. *J. Electroanalyt. Chem.* **1989**, *258*, 193.
(81) Ferrere, S.; Zaban, A.; Gregg, B. A. *J. Phys. Chem. B* **1997**, *101*, 4490.
(82) Sayama, K.; Sugino, M.; Sugihara, H.; Abe, Y.; Arakawa, H. *Chem. Lett.* **1998**, 753.
(83) Wang, Z. S.; Li, F. Y.; Huang, C. H.; Wang, L.; Wei, M.; Jin, L. P.; Li, N. Q. *J. Phys. Chem. B* **2000**, *104*, 9676.
(84) Hara, K.; Horiguchi, T.; Kinoshita, T.; Sayama, K.; Sugihara, H.; Arakawa, H. *Sol. Energy Mater. Sol. Cells* **2000**, *64*, 115.
(85) Chen, H. Y.; Tagore, R.; Das, S.; Incarvito, C.; Faller, J. W.; Crabtree, R. H.; Brudvig, G. W. *Inorg. Chem.* **2005**, *44*, 7661.
(86) Das, S.; Incarvito, C. D.; Crabtree, R. H.; Brudvig, G. W. *Science* **2006**, *312*, 1941.
(87) Duonghong, D.; Borgarello, E.; Grätzel, M. *J. Am. Chem. Soc.* **1981**, *103*, 4685.
(88) Storrier, G. D.; Takada, K.; Abruña, H. D. *Inorg. Chem.* **1999**, *38*, 559.
(89) Whittle, B.; Everest, N. S.; Howard, C.; Ward, M. D. *Inorg. Chem.* **1995**, *34*, 2025.
(90) Beard, M. C.; Turner, G. M.; Schmuttenmaer, C. A. *Phys. Rev. B* **2000**, *62*, 15764.
(91) Baxter, J. B.; Schmuttenmaer, C. A. *J. Phys. Chem. B* **2006**, *110*, 25229.
(92) Limburg, J.; Vrettos, J. S.; Liable-Sands, L. M.; Rheingold, A. L.; Crabtree, R. H.; Brudvig, G. W. *Science* **1999**, *283*, 1524.
(93) McGlynn, S. P.; Vanquickenborne, L. G.; Kinoshita, M.; Carroll, D. G. *Introduction to Applied Quantum Chemistry*; Holt, Rinehart, and Winston Inc.: New York 1972.
(94) Rego, L. G. C.; Batista, V. S. *J. Am. Chem. Soc.* **2003**, *125*, 7989.
(95) Cerdá, j.; Soria, F. *Phys. Rev. B* **2000**, *61*, 7965.
(96) Hoffman, R. *Rev. Mod. Phys.* **1988**, *60*, 601.
(97) *Semiconductor Surfaces and Interfaces*; Mönch, W., Ed.; Springer: Berlin, 1993; Vol. 26.
(98) Kresse, G.; Furthmuller, J. *Vienna ab initio Simulation Package*; 4.4.5 ed.; VASP: Vienna, 2001.
(99) Kresse, G.; Furthmuller, J. *Phys. Rev. B* **1996**, *54*, 11169.
(100) Kresse, G.; Furthmuller, J. *Comp. Mat. Sci.* **1996**, *6*, 15.
(101) Perdew, J. P. In *Electronic Structure of Solids '91*; Ziesche, P., Eschrig, H., Eds.; Akademie Verlag: Berlin, 1991.
(102) Vanderbilt, D. *Phys. Rev. B* **1990**, *41*, 7892.
(103) Dieblod, U. *Surf. Sci. Rep.* **2003**, *48*, 53.
(104) Duncan, W. R.; Prezhdo, O. V. *J. Phys. Chem. B* **2005**, *109*, 365.
(105) Jaguar 5.0; Schrodinger, LLC: Portland, OR, 2002.
(106) Frisch, M. J.; Trucks, G. W.; Schlegel, H. B.; Scuseria, G. E.; Robb, M. A.; Cheeseman, J. R.; Montgomery, J. A., Jr.; Vreven, T.; Kudin, K. N.; Burant, J. C.; Millam, J. M.; Iyengar, S. S.; Tomasi, J.; Barone, V.; Mennucci, B.; Cossi, M.; Scalmani, G.; Rega, N.; Petersson, G. A.; Nakatsuji, H.; Hada, M.; Ehara, M.; Toyota, K.; Fukuda, R.; Hasegawa, J.; Ishida, M.; Nakajima, T.; Honda, Y.; Kitao, O.; Nakai, H.; Klene, M.; Li, X.; Knox, J. E.; Hratchian, H. P.; Cross, J. B.; Bakken, V.; Adamo, C.; Jaramillo, J.; Gomperts, R.; Stratmann, R. E.; Yazyev, O.; Austin, A. J.; Cammi, R.; Pomelli, C.; Ochterski, J. W.; Ayala, P. Y.; Morokuma, K.; Voth, G. A.; Salvador, P.; Dannenberg, J. J.; Zakrzewski, V. G.; Dapprich, S.; Daniels, A. D.; Strain, M. C.; Farkas, O.; Malick, D. K.; Rabuck, A. D.; Raghavachari, K.; Foresman, J. B.; Ortiz, J. V.; Cui, Q.; Baboul, A. G.; Clifford, S.; Cioslowski, J.; Stefanov, B. B.; Liu, G.; Liashenko, A.; Piskorz, P.; Komaromi, I.; Martin, R. L.; Fox, D. J.; Keith, T.; Al-Laham, M. A.; Peng, C. Y.; Nanayakkara, A.; Challacombe, M.; Gill, P. M. W.; Johnson, B.; Chen, W.; Wong, M. W.; Gonzalez, C.; Pople, J. A. *Gaussian 03*; Gaussian, Inc.: Wallingford, CT, 2004.
(107) Moser, J.; Punchihewa, S.; Infelta, P. P.; Grätzel, M. *Langmuir* **1991**, *7*, 3012.
(108) Persson, P.; Bergström, R.; Lunell, S. *J. Phys. Chem. B* **2000**, *104*, 10348.
(109) Moser, J.; Punchihewa, S.; Infelta, P. P.; Gratzel, M. *Langmuir* **1991**, *7*, 3012.
(110) Schmuttenmaer, C. A. *Chem. Rev.* **2004**, *104*, 1759.
(111) Gundlach, L.; Ernstorfer, R.; Willig, F. *Phys. Rev. B* **2006**, *74*.
(112) Turner, G. M.; Beard, M. C.; Schmuttenmaer, C. A. *J. Phys. Chem. B* **2002**, *106*, 11716.
(113) Ramakrishna, G.; Ghosh, H. N. *J. Phys. Chem. B* **2001**, *105*, 7000.
(114) Abuabara, S. G.; Rego, L. G. C.; Batista, V. S. *J. Am. Chem. Soc.* **2005**, *127*, 18234.
(115) Asbury, J. B.; Ellingson, R. J.; Ghosh, H. N.; Ferrere, S.; Nozik, A. J.; Lian, T. Q. *J. Phys. Chem. B* **1999**, *103*, 3110.